International Communications in Heat and Mass Transfer 87 (2017) 228–236

Contents lists available at ScienceDirect

International Communications in Heat and Mass Transfer

journal homepage: www.elsevier.com/locate/ichmt

Comparison of numerical phase-change models through Stefan vaporizing problem

Dae Gon Kim, Chul Hong Jeon, Il Seouk Park*

School of Mechanical Engineering, Kyungpook National University, 1370, Sangyeok-dong, Buk-gu, Daegu 702-701, Republic of Korea

ARTICLE INFO

Keywords:
Stefan problem
Phase-change model
Vaporization

ABSTRACT

In phase-change heat transfer, it is possible that a large amount of heat is transferred with a relatively small flow rate of working fluid because a large amount of latent heat is exchanged during the phase change process. Therefore, the phenomenon is observed in various industries. However, it is difficult to systematically investigate the phenomenon only by experiment, consequently, it is important to conduct a relevant numerical study simultaneously. In the numerical analysis, it is crucial to carefully address the thermofluidic discontinuity at the phase interface. In order to calculate the mass and energy exchange through the phase interface, various methodologies have been proposed, such as utilizing the temperature difference with the saturation temperature or the heat flux around the interface. In this study, based on the VOF method, numerical phase-change models proposed by Lee, Rattner et al., and Sun et al. were investigated and compared through the Stefan vaporization problem.

1. Introduction

Phase change is the phenomenon of modification of a fluid's physical phase caused by thermal conditions. Because a large amount of latent heat is transferred during the phase changing process, it is feasible that a large amount of thermal energy is transferred at a relatively small flow rate. Therefore, the phase changing phenomenon has been widely applied in various industrial applications such as power plants, refrigeration systems, desalination plants etc. However, because the shape of the phase interface continuously deforms as a result of heat transfer and the deformation is significantly chaotic in certain cases, numerical or analytical approach has been applied to limitedly simple phase-changing problems and a significant number of the previous studies of phase-change heat transfer has largely been carried out by the experimental approach notwithstanding the high costs. A variety of experimental techniques using high-speed camera, infrared image processing, and transparent electrode heater have been developed over the last decade. Because of this technical development, it has become possible to explore the phenomenon at a deeper physical consideration.

The demand for direct numerical analysis of the phase changing process, however, is still increasing because of the advantage that it allows one to observe the inside of the phenomenon without any artificial interference. However, because of the complexities of the phenomenon and resulting high computing costs, numerical studies are limited to highly straightforward phase-changing problems; moreover, there never a consensus on the accuracy of the numerical solution. To enable the use of numerical tools for the purpose of reproducing the existing experimental results as well as solving a variety of phase changing situations appearing in real engineering problems, the characteristics of the numerical model for phase changing process must be examined in advance through a simple phase-change problem.

A number of numerical phase-change models have been presented and are steadily undergoing modifications. The existing numerical phase-change models can be classified into models using the difference between cell temperature and saturation temperature (Lee [1] and Rattner et al. [2]) and models using the heat flux data around the interface cell (sharp interface model [3] and Sun et al. [4]). All of these phase-change models predict the phase change amount using the heat transfer information, and consider the energy source as the latent heat relevant to the mass change in the interface cell when solving the energy conservation.

In the case of the Lee model [1], which has been widely used because of its simplicity, the inconsistency of the numerical coefficient that directly affects the prediction of the amount of phase change poses a challenge. It was reported that a wide range of this coefficient—from 10^{-1} to 10^{8} [5–10]—was applied on a case-by-case basis. Meanwhile, Rattener et al. [2] proposed a new model that includes the computing time interval for predicting the phase change amount. They suggested the maximum allowable time step size considering thermal diffusion stability. Sun et al. [4] developed a new numerical phase-change model

* Corresponding author at: School of Mechanical Engineering, Kyungpook National University, 80, Daehakro, Bukgu, Daegu 41566, Republic of Korea.
E-mail address: einstein@knu.ac.kr (I.S. Park).

http://dx.doi.org/10.1016/j.icheatmasstransfer.2017.07.013

that is a control-volume-based sharp interface model, which predicts the phase change amount using the heat flux data in the computational cell including the gas-liquid interface.

In this study, the existing Lee, Rattner, and Sun models are applied to the one-dimensional Stefan vaporization problem that does not include nonlinear convection terms and thus has a simple exact solution [3,11,12]. First, the characteristics of each model will be briefly introduced. The dependency of the numerical coefficient for the Lee model and time step dependency of the Rattner model will be addressed. The time progressions in the position of the phase interface are compared between the phase-change models. Error analysis using the exact solution will be introduced.

2. Numerical analysis

2.1. Governing equations

For the one-dimensional Stefan problem, the conservation equations of volume fraction and energy after omitting the convection terms are used as a governing equation set:

$$\frac{\partial \alpha_v}{\partial t} = \frac{\dot{m}_v}{\rho_v} \tag{1}$$

$$\frac{\partial}{\partial t}(\rho h) = \nabla\cdot(\lambda \nabla T) + S \tag{2}$$

where α is volume fraction, t is time, $\dot{m}$ is mass change rate per unit volume, ρ is density, h is enthalpy, λ is thermal conductivity, T is temperature, S is energy source per unit volume, and subscripts v and l represent vapor and liquid respectively.

The enthalpy of the interface cell where the vapor and liquid coexist defined by the following Eq. (3):

$$h = \frac{\alpha_v \rho_v h_v + \alpha_l \rho_l h_l}{\alpha_v \rho_v + \alpha_l \rho_l} \tag{3}$$

where h_l and h_v are defined by Eqs. (4) and (5), respectively, and T_{sat} represents the saturation temperature.

$$h_l = C_{p,l}(T - T_{sat}) \tag{4}$$

$$h_v = C_{p,v}(T - T_{sat}) \tag{5}$$

where C_p is the specific heat under constant pressure condition.

The values of density and thermal conductivity applied in the energy conservation Eq. (2) are the weighted averages determined using the volume fraction of each phase.

$$\rho = \alpha_v \rho_v + \alpha_l \rho_l \tag{6}$$

$$\lambda = \alpha_v \lambda_v + \alpha_l \lambda_l \tag{7}$$

The $\dot{m}$ (mass change rate per unit volume) and S (energy source per unit volume) in the governing Eqs. (1) and (2) are differently obtained for each phase-change model.

2.2. Phase-change models

2.2.1. Lee model

In the Lee model, the mass change rate per unit volume is obtained using the difference between the cell temperature and saturation temperature and the volume fraction following Eq. (8):

$$\begin{cases} \dot{m}_v = -\dot{m}_l = r\alpha_l \rho_l \frac{T - T_{sat}}{T_{sat}} & \text{(for vaporization)} \\ \dot{m}_l = -\dot{m}_v = r\alpha_v \rho_v \frac{T - T_{sat}}{T_{sat}} & \text{(for condensation)} \end{cases} \tag{8}$$

where r is a numerical coefficient with s^{-1} dimensions. As mentioned previously, significantly different values of r were used on a case-by-case basis. A few researchers defined r as the mass transfer time relaxation [13] or empirical coefficient [8].

In actuality, the temperature at the phase interface is to be maintained as the saturation temperature. However, as the numerical simulation progresses, the cell temperature in the interface cell tends to deviate significantly from the saturation temperature as a result of the heat transfer between the saturated and unsaturated phases. To compensate for this and maintain the cell temperature of the interface cell to be equal to the saturation temperature, the energy source term is added to the right-hand side of energy conservation Eq. (2). Its magnitude is determined by the following Eq. (9):

$$S = \begin{cases} -|\dot{m}|\, h_{lv} & \text{(for vaporization)} \\ |\dot{m}|\, h_{lv} & \text{(for condensation)} \end{cases} \tag{9}$$

where h_{lv} is the latent heat for the phase change.

2.2.2. Rattner model

To overcome the solution's dependency on the numerical coefficient in the Lee model, the following phase-change model was proposed by Rattner et al. [2].

$$S = \begin{cases} -\min(S_1,\ S_2,\ S_3) & \text{(for vaporization)} \\ \min(S_1,\ S_2,\ S_3) & \text{(for condensation)} \end{cases} \tag{10}$$

where, S_1, S_2, and S_3 are defined as follows.

$$S_1 = \left| \frac{(\rho C_p)_{eff}(T - T_{sat})}{\Delta t} \right| \tag{11}$$

$$S_2 = \begin{cases} \frac{\alpha_l \rho_l h_{lv}}{\Delta t} & \text{(for vaporization)} \\ \frac{\alpha_v \rho_v h_{lv}}{\Delta t} & \text{(for condensation)} \end{cases} \tag{12}$$

$$S_3 = \frac{h_{lv}}{\Delta t}\left(\frac{1}{\rho_v} - \frac{1}{\rho_l}\right)^{-1} \tag{13}$$

The parameter S_1 is the magnitude of the heat source calculated from the phase change amount for a single computing time interval (Δt); the phase change amount is obtained from the deviation between the cell temperature and saturation temperature. The parameter S_2 represents the limit of the energy source because it is not practicable for the phase change amount exceed the amount of the saturated phase remaining in the cell. The parameter S_3 is a device for numerical stability that limits the growth rate of the interface and is known as the Cournat-Friedrichs-Lewy (CFL) condition.

The mass change rate per unit volume to be applied to the volume fraction conservation Eq. (1) is calculated by the following Eq. (14).

$$\dot{m}_v = -\dot{m}_l = -\frac{S}{h_{lv}} \tag{14}$$

This model successfully removed the ambiguous numerical coefficient in the Lee model; however, there is a likelihood of time step dependency because of the inclusion of the computing time interval for obtaining the phase change amount, as illustrated in Eqs. (11)–(13). Rattner et al. [2] suggested the following maximum allowable time step size considering the thermal diffusion stability:

$$\Delta t \le \frac{1}{6}\left[\Delta x^2 \Big/ \left(\frac{\lambda}{\rho C_p}\right)_{eff}\right] \tag{15}$$

where Δx is the grid size.

In this study, when applying the various time step sizes, the accuracy of this model is addressed through one-dimensional Stefan problem.

2.2.3. Sun model

To overcome the dependency of the numerical coefficient for the Lee model and time step size for the Rattner model, Sun et al. [4] suggested the numerical phase-change model that uses the total heat

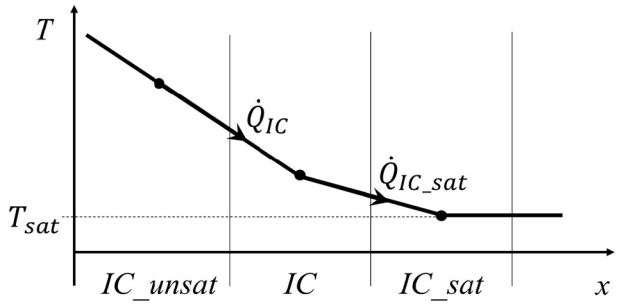

Fig. 1. Definition for computing cells and heat fluxes in the Sun model.

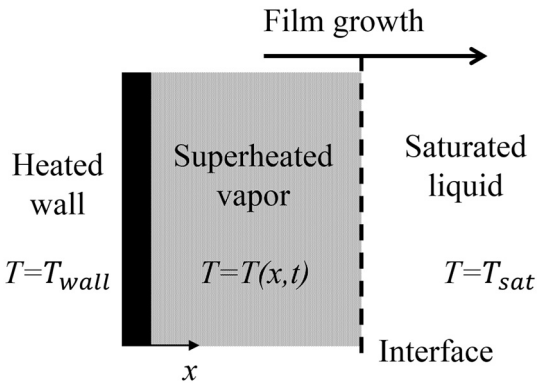

Fig. 2. Schematic of one-dimensional Stefan vaporization problem.

Table 1
Properties of isobutane.

Property	Liquid	Vapor
$\rho\ [kg\,m^{-3}]$	550.6	9.12
$k\ [W\,m^{-1}\,K^{-1}]$	0.0892	0.0169
$C_p\ [J\,kg^{-1}\,K^{-1}]$	2446	1819
$h_{lv}\ [J\,kg^{-1}]$	329,365	
$\sigma\ [kg\,s^{-2}]$	0.01	

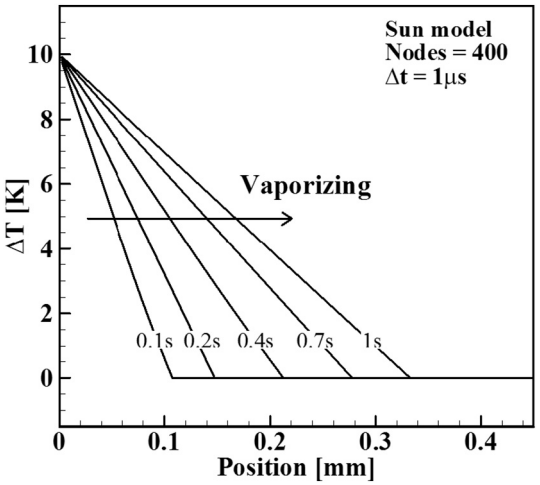

Fig. 3. Temperature profiles over time by the Sun model.

transfer amount in the interface cell instead of the temperature difference which was used in the previous two models. Thus, it could be considered as a control-volume-based sharp interface model.

In this model, the mass change rate per unit volume is obtained from the heat transfer amount through the cell faces as expressed by following Eq. (16):

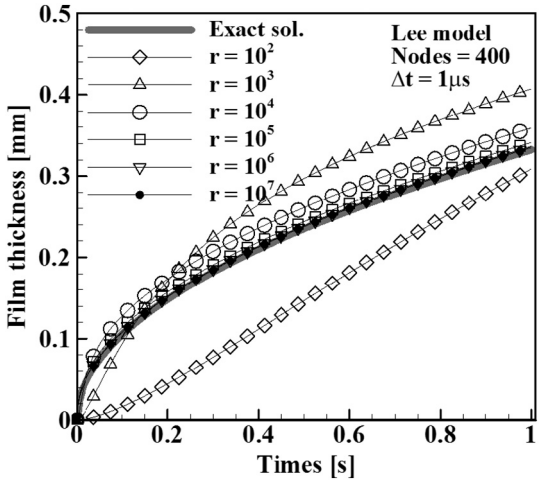

Fig. 4. Position of phase interface by the Lee model with different numerical coefficients.

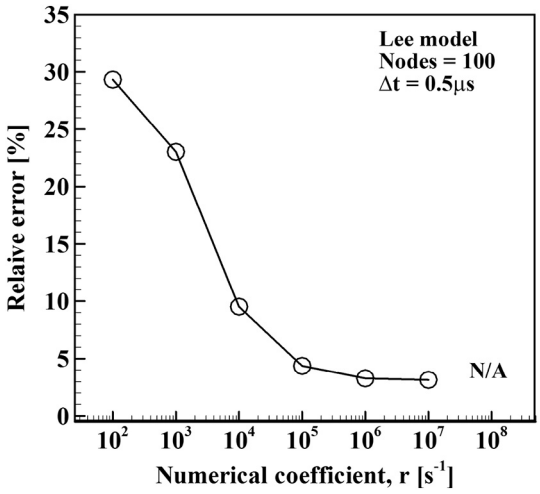

Fig. 5. Relative errors in the position of phase interface with increasing numerical coefficient in the Lee model.

$$\dot{m}_v = -\dot{m}_l = \frac{\dot{Q}_{IC}}{h_{lv} V_{IC}} + \frac{\dot{Q}_{IC,sat}}{h_{lv} V_{IC,sat}} \tag{16}$$

where, V is cell volume, subscript IC represents the interface cell including the phase interface, and IC_sat and IC_unsat represent the neighboring cells of IC cell on the saturated and unsaturated phases, respectively. The $\dot{Q}_{IC}$ is the heat transfer amount between the IC and IC_unsat cells, as illustrated in Fig. 1. The heat influx $\dot{Q}_{IC}$ from the IC_unsat cell to the IC cell is considered to be positive; the $\dot{Q}_{IC}$ in the opposite direction has a negative value. The $\dot{Q}_{IC\_sat}$ is the heat transfer amount between the IC and IC_sat cells and is positive when the heat influx is from the IC cell to the IC_sat cell.

Meanwhile, the energy source term added to the right-hand side of the energy conservation Eq. (2) is obtained using only $\dot{Q}_{IC}$ as described by the following Eq. (17).

$$S = -\frac{\dot{Q}_{IC}}{V_{IC}} \tag{17}$$

Sun et al. proposed a slightly complex expression (Eq. (16)) for the mass change rate because the cell temperature in the interface cell is not maintained at the saturation temperature during computation. In actuality, the temperature at the phase interface is maintained at the saturation temperature during the phase change, the thermal gradient exists only in the unsaturated phase, and the saturation temperature is kept constant in the whole saturated phase area. However, during

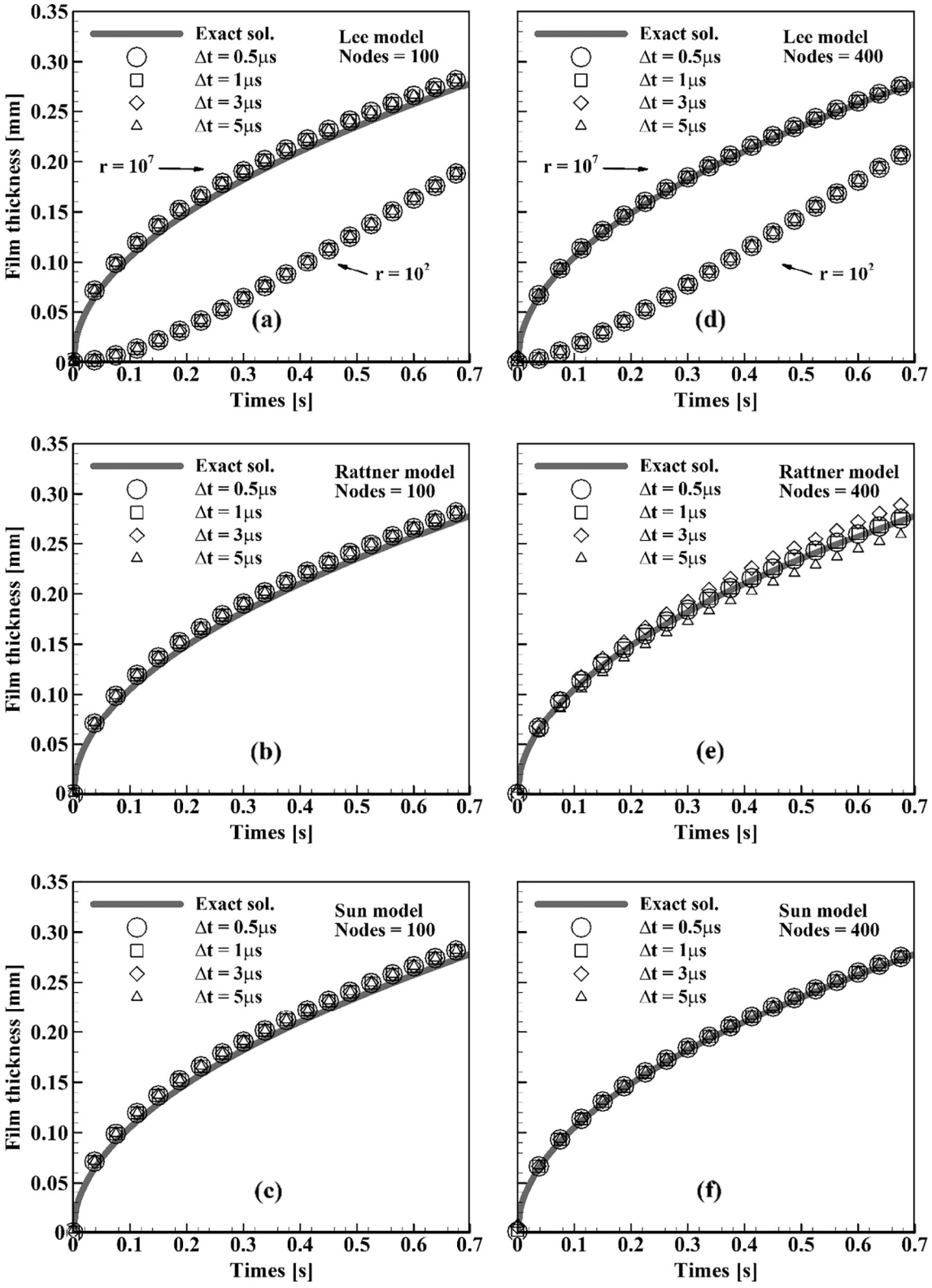

Fig. 6. Position of phase interface for various time step sizes for the different models and numbers of node.

numerical simulation of the phase change, the cell temperature is not adequately maintained at the saturation temperature notwithstanding the application of the energy source such as Eqs. (9), (10), and (17) (In the models that use the temperature difference, such as the Lee and Rattner models, in the absence of temperature deviation, it is not feasible for the calculation to proceed as can be observed from Eqs. (8) and (11)). Therefore, if the phase change amount is obtained using the net heat balance in the interface cell or the heat transfer with only the unsaturated phase, a significant error could occur in predicting the phase change amount. In order to overcome such possible inconsistency, Sun et al. proposed Eq. (16), which simultaneously uses the heat transfer data at the interface cell and the cell in the immediate

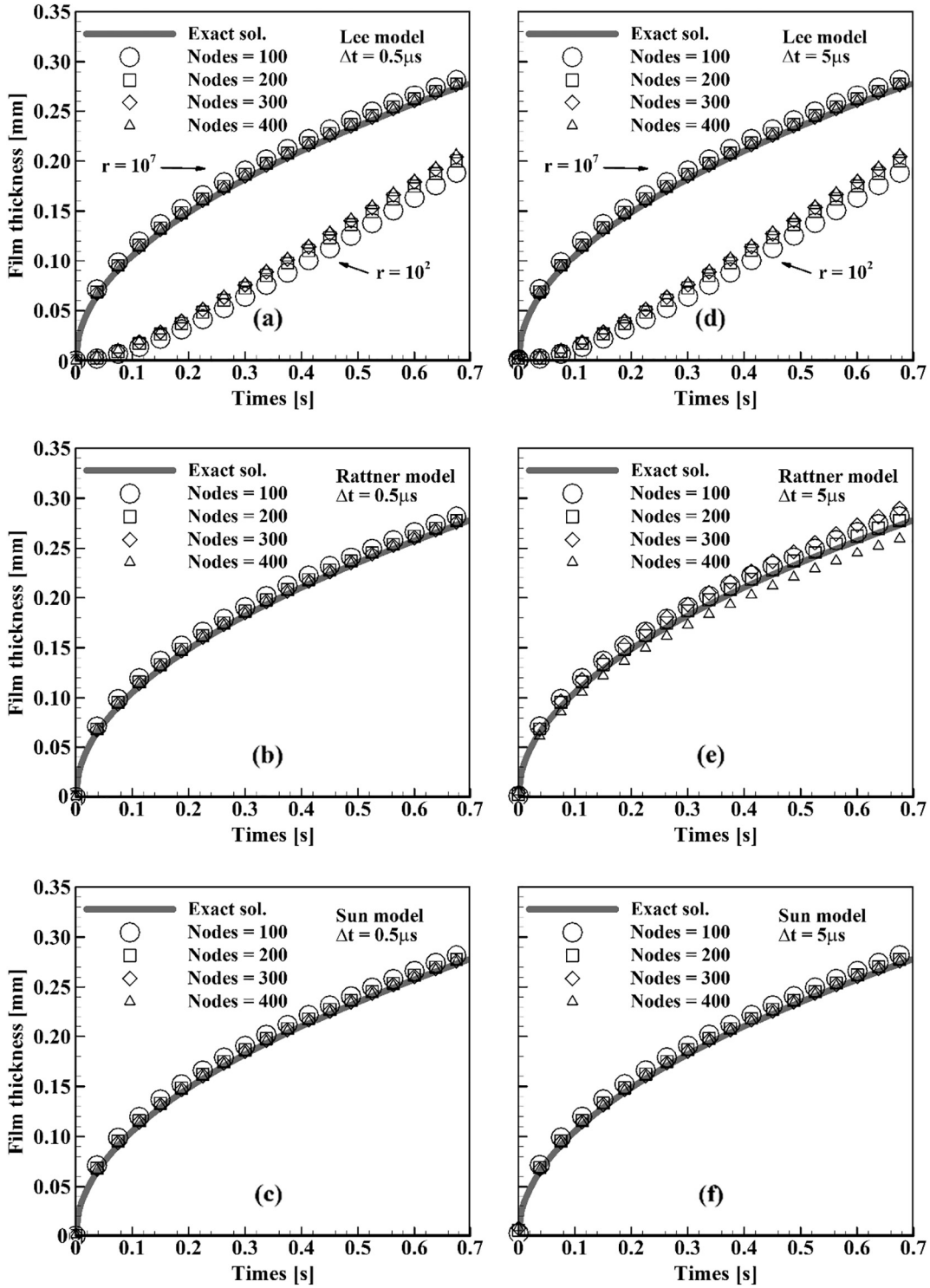

Fig. 7. Position of phase interface for various grid systems for the different models and time step sizes.

neighborhood of the saturated phase.

2.3. Numerical scheme

The volume fraction obtained by solving the Eq. (1) affects the unsteady term on the left-hand side of the energy conservation Eq. (2). Conversely, the information on temperature or heat flux obtained from the energy conservation Eq. (2) affect the mass change rate per unit volume on the right-hand side of the volume fraction conservation Eq. (1). Thus, the two equations are 2-way-coupled. Therefore, iterative calculation between the equations is required. However, most of the numerical analyses for phase-change problems adopt an explicit analysis of the volume fraction to avoid an excessive increase in computing cost.

In this study, to characterize the various numerical phase-change models, similar numerical procedure is applied. First, an explicit analysis is performed on the volume fraction Eq. (1); thus, the mass change rate per unit volume on the right-hand side of Eq. (1) is calculated using the values at the previous time step, as expressed in following Eq. (18).

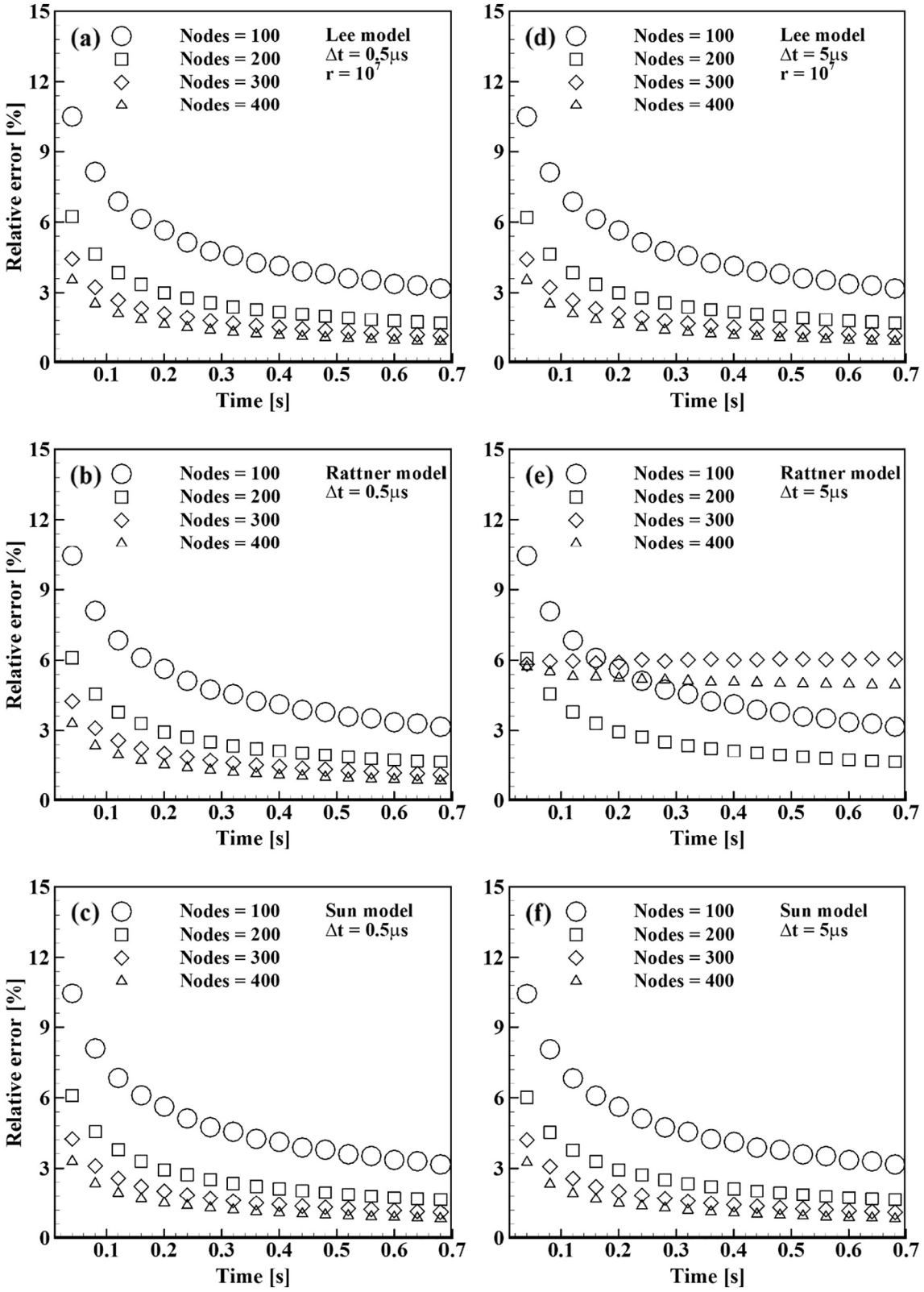

Fig. 8. Relative error for various grid systems for the different models and time step sizes.

$$\dot{m} = \dot{m}(\alpha^{old}, T^{old}, \dot{Q}^{old}) \tag{18}$$

Next, for energy conservation, matrix-type simultaneous equations are solved. The first term (thermal diffusion term) on the right-hand side of the energy conservation Eq. (2) is dealt with implicitly using the temperature in the present time step; the second term (energy source term) is handled explicitly using the mass change rate per unit volume of Eq. (18) used in solving Eq. (1). A source term linearization technique is not applied; therefore, there is no iteration between the governing equations and no local iteration for the energy conservation equation at each time step.

Table 2
Calculation time and error for the three models.

Nodes	Δt[μs]	Lee model (r = 10^7)		Rattner model		Sun model	
		Calc. time[s]	Error [%]	Calc. time[s]	Error [%]	Calc. time[s]	Error [%]
400	0.5	13,505	0.885311	12,050	0.791539	13,464	0.820908
	1	6105	0.885277	6983	0.824866	6767	0.819956
	3	2309	0.880944	2258	5.734047	2372	0.809382
	5	1368	0.885194	1209	4.930912	1356	0.813467
300	0.5	12,191	1.135515	10,140	1.092534	12,310	1.087235
	1	6062	1.135477	5564	1.057993	6263	1.086559
	3	1961	1.131046	1997	3.243662	2047	1.076308
	5	1188	1.135339	1186	6.046316	1244	1.081148
200	0.5	11,690	1.645477	10,139	1.617676	11,901	1.612982
	1	5920	1.645438	5529	1.618349	5535	1.612624
	3	1910	1.640941	1956	1.620981	1990	1.603235
	5	1156	1.645233	1183	1.619764	1209	1.609327
100	0.5	10,736	3.141285	9550	3.129294	10,081	3.125067
	1	4800	3.14125	5392	3.129696	5296	3.12485
	3	1595	3.136711	1804	3.131078	1898	3.116332
	5	831	3.140989	1099	3.128614	822	3.123185

3. Results and discussions

In this study, to analyze the accuracy of three numerical phase-change models introduced previously, the various grid systems and time step sizes are applied to the one-dimensional Stefan vaporization problem, and the characteristics of each numerical phase-change model are compared. Fig. 2 shows the schematic diagram of the one-dimensional Stefan problem. Initially, the whole computing domain is filled with the liquid at a saturation temperature. The liquid begins to vaporize because of the influence of the left wall, which is maintained at a constant temperature higher than the saturation temperature. Therefore, superheated vapor and saturated liquid exist on the left and right of the phase interface, respectively.

The working fluid used in this study is isobutane; the thermal properties such as thermal conductivity of each phase and latent heat are listed in Table 1. The saturation temperature is 298 K and wall temperature is 308 K. The whole computing domain is up to 2 mm from the wall.

Because the Stefan problem does not include any nonlinear convection terms, the exact solution could be obtained using following Eq. (19), which is used as a reference for error analysis of each phase-change model:

$$\delta_{an}(t) = 2\varepsilon\sqrt{\frac{\lambda_b t}{\rho_v C_{p,v}}} \tag{19}$$

$$\varepsilon \exp(\varepsilon^2)\, erf(\varepsilon) = \frac{C_{p,v}(T_{wall} - T_{sat})}{h_{lv}\sqrt{\pi}} \tag{20}$$

where ε is a solution of transcendental equation and erf is an error function.

Fig. 3 is the result from the Sun model and shows the temperature change inside the domain over time. Four hundred gird cells are applied, and the time step size is 1 μs. In the superheated vapor area on the left, a nearly linear decrease in temperature from the wall temperature to saturation temperature is observed. The temperature in the saturated region on the right is adequately maintained at the saturation temperature.

Fig. 4 presents the results by the Lee model of using 400 grids and time step size of 1 μs. The time change of interfacial position is plotted for the six numerical coefficients from 10^2 to 10^7. A very different interface growth rate is predicted depending on the size of r. However, as the value of r increases, the interface growth pattern gradually converges to the exact solution. As can be expected from Eq. (8), the increase of the numerical coefficient may have a risk of excessively accelerating the interface growth rate. However, in actuality, as the value of r increases, the interface growth rate is relaxed again and converges to an exact solution. For the cases of small numerical coefficient, the interface growth rate is very slow at the beginning and becomes faster than the exact solution over time. On the other hand, when a large numerical coefficient is applied, the interface grows rapidly at the beginning; however, its growth rate reduces over time.

Fig. 5 plots the relative error of the position of phase interface at 0.7 s while increasing the numerical coefficient. The relative error is defined as the value obtained by dividing the difference between the phase interface positions obtained from the present simulation and exact solution, by the exact position. The relative error rapidly reduces as the numerical coefficient increases up to 10^7; however, if r increases to 10^8 or higher, the solution diverges. This implies that it is necessary to increase the numerical coefficient to obtain a more precise result; however, the excessively large numerical coefficient does not guarantee the convergence and accuracy of the result. Furthermore, the maximum numerical coefficient that guarantees the solution convergence differs on a case-by-case basis. This is a key disadvantage of the Lee model.

Fig. 6 shows the interface growth patterns when applying different phase-change models. The results for the 100 and 400 grid systems and time step sizes of 0.5, 1, 3, and 5 μs are presented. In Fig. 6 (a) and (b)

Table 3
Calculation time and error for different numerical coefficients in the Lee model.

Nodes	Δt [μs]	r (Lee model)									
		10^2		10^3		10^4		10^5		10^6	
		Calc. time[s]	Error [%]	Calc. time[s]	Error [%]	Calc. time[s]	Error [%]	Calc. time[s]	Error [%]	Calc. time[s]	Error [%]
400	0.5	13,210	22.76	13,197	25.06	13,047	9.474	13,315	3.176	13,330	1.299
	1	5952	22.76	5983	25.06	5898	9.474	6001	3.176	6105	1.299
	3	2352	22.78	2313	25.05	2353	9.466	2354	3.168	2370	1.292
	5	1420	22.76	1381	25.06	1410	9.473	1412	3.175	1426	1.299
300	0.5	11,849	23.52	11,775	24.81	11,666	9.442	12,033	3.255	11,874	1.487
	1	5888	23.52	5945	24.81	5866	9.442	5977	3.255	6001	1.487
	3	1992	23.54	1942	24.80	2000	9.434	1988	3.248	2065	1.480
	5	1219	23.52	1192	24.81	1204	9.441	1218	3.255	1267	1.487
200	0.5	11,340	25.02	11,260	24.34	11,127	9.410	11,441	3.470	11,517	1.904
	1	5798	25.02	5832	24.34	5764	9.410	5827	3.470	5812	1.904
	3	1939	25.03	1880	24.33	1931	9.402	1933	3.463	2007	1.900
	5	1180	25.02	1130	24.34	1159	9.410	1161	3.470	1198	1.904
100	0.5	10,337	29.33	10,346	23.02	10,234	9.521	10,344	4.369	10,515	3.278
	1	4727	29.33	4778	23.02	4699	9.521	4772	4.369	4846	3.278
	3	1628	29.34	1559	23.02	1614	9.514	1615	4.362	1762	3.271
	5	863	29.33	854	23.02	848	9.521	857	4.369	901	3.278

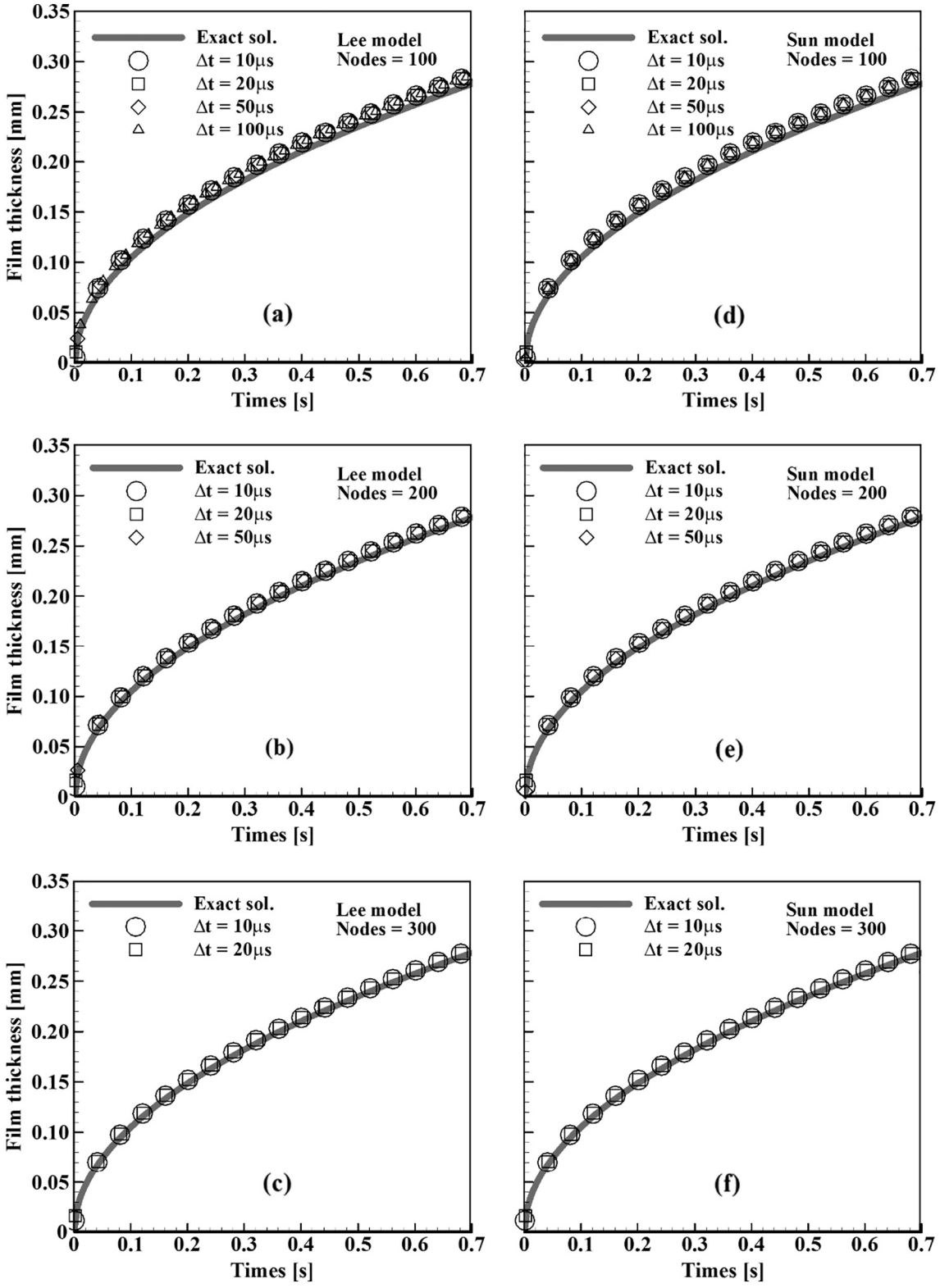

Fig. 9. Position of phase interface for larger time step sizes in the Lee and Sun models.

for the Lee model, the results for two different numerical coefficients, 10^2 and 10^7 are compared simultaneously. Even if the time step size varies 10 fold from 0.5 to 5 μs, highly similar interface growth patterns are predicted if the same numerical coefficient is applied. Although the results of $r = 10^2$ is completely different from an exact value, the solution dependency on the time step size does not appear. For the cases of numerical coefficient of 10^7 much closer to the exact solutions, the denser grid cases of 400 nodes in Fig. 6 (b) illustrate improved agreement with an exact solution. Next, in Fig. 6 (c) and (d) for the Rattner model, the solution dependency on the time step size appears for 400 grid cases. However, the 100 grid cases do not demonstrate similar time step dependency. This is because the maximum allowable time step size of Eq. (15) proposed by Rattner et al. [2] is directly affected by the grid size. By Eq. (15), the allowable time step sizes are 65.4 and 4.09 μs for

the 100 and 400 grids, respectively. However, in the present problem, it is revealed that a time step size smaller than 1 μs is required for the 400 grids. On the other hand, in Fig. 6 (e) and (f) where the Sun model is applied, no time step dependency is apparent, and the denser grid cases predict more accurate interface growth patterns.

To examine the grid size dependency for each model, the interface growth patterns for the cases of the number of grids of 100, 200, 300, and 400 are compared in Fig. 7. As illustrated in Fig. 7 (a) and (b), it is apparent that the Lee model has a more considerable grid size dependency while applying a smaller numerical coefficient. As described above, there is negligible dependency on the time step size in the Lee model. For the Rattner model, the grid size dependency is not significant for the case of small time step size of 0.5 μs as illustrated in Fig. 7 (c); however, it becomes highly significant for the case of large time step size of 5 μs as illustrated in Fig. 7 (d). On the other hand, in Fig. 7 (e) and (f) for the Sun model, the grid size dependency is not severe with no regard to the time step size applied.

Fig. 8 shows the relative error of the interface position at 0.7 s in comparison with the exact solution. Fig. 8 (a), (b), and (c) illustrate the results for the time step size of 0.5 μs, and Fig. 8 (d), (e) and (f) do so for the time step size of 5 μs. Overall, the relative error is decreasing over time. For the cases of 0.5 μs, as the number of grid increases, the relative error is reduced without any significant difference between the models. Meanwhile, for the cases of 5 μs in Fig. 8 (d), (e), and (f), the Lee model and Sun model illustrate patterns which are highly similar to those of 0.5 μs cases; however, the Rattner model reveals a slight difference; the relative error patterns for the cases of number of grids 300 and 400, which do not satisfy the allowable time step size condition, are considerably deviated from those of 0.5 μs cases.

Table 2 lists the relative error in the interfacial position and computing time up to 0.7 s for the cases of various numbers of grid and time step sizes for different numerical phase-change models. First, the run time varies negligibly with phase-change model because there is no iterative calculation of governing equations and local iteration of energy conservation equation. The run time meaningfully varies depending only on the number of grid and time step size applied. The relative error of the Lee model is not significantly affected by the time step size and becomes smaller as the number of cell increases. On the other hand, for the cases of the Rattner model, the relative error varies considerably depending on both the time step size and number of grid; however, if the time step size is sufficiently smaller than the allowable time step size for the applied grid size, the relative error is not affected by the time step size. For the Sun model, no significant variation in the relative error according to the time step size is apparent for any of the cases of the number of girds, which is similar to the Lee model. For the Lee model and Sun model, each computing case reveals reduced relative errors with the application of a denser grid.

Table 3 lists the run time and relative error for different numbers of grid and time step sizes with increasing numerical coefficient from 10^2 to 10^6 in the Lee model. As a departure from claims by previous researchers, no increase in run time is observed with increasing the numerical coefficient. By increasing the numerical coefficient or numbers of grid, a higher accuracy of the solution is obtained. On the other hand, it is revealed that the time step size does not affect the solution accuracy.

We simulate the Lee model and Sun model, which have not revealed any time step size dependency for the values 0.5–5 μs tested so far, with significantly larger time step size (up to 200 fold larger) than the previous ones. As illustrated in Fig. 9 (a) and (d), for the case of grid 100, although the time step size is increased to 100 μs, the time step size dependency does not appear. However, in Fig. 9 (b) and (e) for the grid 200, the time step size of 100 μs could not provide a converged solution. This is caused by the fact that the time step size of 100 μs is beyond the CFL condition required for numerical stability. The rest of the time step sizes (10, 20, and 50 μs) still reveal no time step dependency. In Fig. 9 (c) and (f) for grid 300, a solution divergence is detected for time step size of 50 μs or larger; no time step dependency is observed for time step size smaller than 50 μs.

4. Conclusions

In numerical analyses for unsteady flows, the solution dependency on both the time step and grid sizes must be examined simultaneously. Moreover, in the problems where the phase interface moves through the grid interfaces, if a denser gird system is applied to get a higher resolution of results, a much smaller time step size is required; therefore, a more careful consideration is required for determining the grid and time step sizes. In particular, for the phase-change heat transfer problems, it is necessary to review in advance the characteristic of the numerical phase-change model applied. In this study, three different phase-change models were applied to the one-dimensional Stefan vaporization problem, and the solution's dependency on the grid and time step sizes was examined. The three models had the commonality that they can achieve higher solution accuracy with the application of a denser grid. However, with respect to the time step size, the Rattner model required a significantly smaller time step size than the CFL condition; otherwise, a more or less large error occurred. In actuality, it was also smaller than the allowable time step size of Eq. (15) determined by considering diffusion stability. On the other hand, the Lee model had a severe solution dependency on the numerical coefficient for predicting the phase change amount. A larger numerical coefficient yielded higher solution accuracy. However, an excessively large numerical coefficient caused the solution to diverge. In both the Lee model and Sun model, no time step size limit was apparent; however, it was necessary to limit the time step size to the level of CFL condition required for numerical stability.

Acknowledgements

This research was supported by the Basic Science Research Program through the National Research Foundation of Korea (NRF), funded by the Ministry of Education (Grant 2016R1D1A1B03934159).

References

[1] W.H. Lee, A pressure iteration scheme for two-phase flow modeling, in: T.N. Veziroglu (Ed.), Multiphase Transport Fundamentals, Reactor Safety, Applications, Hemisphere Publishing, Washington DC, 1980.
[2] A.S. Rattner, S. Garimella, Simple mechanistically consistent formulation for volume-of-fluid based computations of condensing flows, J. Heat Transf. 136 (7) (2014) 071501.
[3] Y. Sato, B. Niceno, A sharp-interface phase change model for a mass-conservative interface tracking method, J. Comput. Phys. 249 (2013) 127–161.
[4] D. Sun, J. Xu, Q. Chen, Modeling of the evaporation and condensation phase-change problems with FLUENT, Numer. Heat Transfer B 66 (2014) 326–342.
[5] H.L. Wu, X.F. Peng, P. Ye, Y.E. Gong, Simulation of refrigerant flow boiling in serpentine tubes, Int. J. Heat Mass Transf. 50 (2007) 1186–1195.
[6] A. Alizadehdakhel, M. Rahimi, A.A. Alsairafi, CFD modeling of flow and heat transfer in a thermosyphon, Int. Commun. Heat Mass Transfer 37 (2010) 312–318.
[7] Z. Yang, X.F. Peng, P. Ye, Numerical and experimental investigation of two phase flow during boiling in a coiled tube, Int. J. Heat Mass Transf. 51 (2008) 1003–1016.
[8] C. Fang, M. David, A. Rogacs, K. Goodson, Volume of fluid simulation of boiling two-phase flow in a vapor-venting microchannel, Front. Heat Mass Transfer 1 (2010) 1–11.
[9] H. Lee, C.R. Kharangate, N. Mascarenhas, I. Park, I. Mudawar, Experimental and computational investigation of vertical downflow condensation, Int. J. Heat Mass Transf. 85 (2015) 865–879.
[10] E.D. Riva, D.D. Col, S.V. Garimella, A. Cavallini, The importance of turbulence during condensation in a horizontal circular minichannel, Int. J. Heat Mass Transf. 55 (2012) 3470–3481.
[11] G. Son, V.K. Dhir, Numerical simulation of film boiling near critical pressures with a level set method, J. Heat Transf. 120 (1998) 183–192.
[12] S.W.J. Welch, J. Wilson, A volume of fluid based method for fluid flows with phase change, J. Comput. Phys. 160 (2000) 662–682.
[13] Q. Liu, J. Yang, W. Qian, H. Gu, M. Liu, Numerical study of the forced convective condensation on a short vertical plate, Heat Transfer Eng. 38 (2017) 103–121.